PROCEEDINGS OF SCIENCE

Nucleon form factors from Nf=2+1+1 twisted mass fermions at the physical point

Constantia Alexandrou
Department of Physics, University of Cyprus, P.O. Box 20537, 1678 Nicosia, Cyprus and Computation-based Science and Technology Research Center, The Cyprus Institute, 20 Konstantinou Kavafi Str., 2121 Nicosia, Cyprus
E-mail: alexand@ucy.ac.cy

Simone Bacchio
Department of Physics, University of Cyprus, P.O. Box 20537, 1678 Nicosia, Cyprus
E-mail: s.bacchio@hpc-leap.eu

Martha Constantinou*
Department of Physics, Temple University, Philadelphia, PA
E-mail: marthac@temple.edu

Kyriakos Hadjiyiannakou, Giannis Koutsou
Computation-based Science and Technology Research Center, The Cyprus Institute, 20 Konstantinou Kavafi Str., 2121 Nicosia, Cyprus
E-mail: k.hadjiyiannakou@cyi.ac.cy, g.koutsou@cyi.ac.cy

Karl Jansen
NIC, DESY, Platanenallee 6, D-15738 Zeuthen, Germany
E-mail: karl.jansen@desy.de

Alejandro Vaquero
Department of Physics and Astronomy, University of Utah, Salt Lake City, UT
*E-mail:*alexvaq@physics.utah.edu

In this proceedings we present results on the nucleon electromagnetic and axial form factors of both the connected and disconnected light and strange quarks contributions. The simulations are performed using a large volume ensemble (5.12 fm) ensemble of N_f=2+1+1 twisted mass fermions with a clover term, and the quark masses fixed to their physical values. Various analysis techniques such as the single-state, two-state and summation fits have been employed to control possible excited states contamination. The momentum dependence of the electromagnetic form factors is fitted to extract the magnetic moment and the electric and magnetic radii.

The 36th Annual International Symposium on Lattice Field Theory - LATTICE2018
22-28 July, 2018
Michigan State University, East Lansing, Michigan, USA.

*Speaker.

PoS(LATTICE2018)142

1. Introduction

Among the frontiers of Nuclear and Particle Physics is the study of the immensely rich and complex structure of the nucleon, both experimentally and theoretically. Of particular interest are the electromagnetic form factors of the nucleon that provide information on the charge and magnetic distributions of the hadrons, that are well-studied experimentally for more that half a century. In particular, the proton electric form factor has been accurately measured, while the neutron electric form factor is less precise as it is extracted from electron-deuteron or electron-helium scattering. The axial form factors are also important probe of the nucleon structure, but their dependence on the momentum transfer is less-known experimentally compared to the electromagnetic form factors. One method to access the axial form factor is by using elastic scattering of neutrinos and protons, or via analyses of charged pion electro-production data off the proton. The induced pseudo-scalar form factor is even more challenging to measure experimentally, which has been determined only at limited values of the momentum transfer from the longitudinal cross section in pion electro-production. In addition, the strange quark contributions, which are subdominant compared to the light quark contributions, are particularly challenging to measure.

Despite the intense experimental activity, there is a need to evaluate form factors theoretically from first principles. Lattice QCD is an ideal formulation for computing hadron charges and form factors, and may provide results that have controlled systematics uncertainties. The field of Lattice QCD has made important progress with simulations at physical values of the quark masses, eliminating the need for a chiral extrapolation, which brings in uncontrolled systematic uncertainties for the baryonic sector.

In this work we present results for the electromagnetic and axial form factors using an ensemble with two degenerate light quarks, strange and charm quarks in the sea (N_f=2+1+1), all of the them fixed to their physical value. We study both the isovector and isoscalar combinations as well as the strange form factors, which receive purely disconnected contributions.

2. Lattice Methodology

The calculation is performed using a lattice formulation that consists of the twisted mass fermion action with a clover term and Iwasaki improved gluon action. This formulation has the advantage of automatic $\mathcal{O}(a)$ improvement once tuned to maximal twist [1]. The lattice volume of the ensemble is $64^3\times128$ (L=5.18 fm) with $m_\pi L$=3.62 [2], and the pion mass around 138 MeV.

In the connected diagram we use sequential inversions through the sink that fixes the separation between the source and sink (t_s), the projector and the sink momentum $\vec{p}\,'$. The results are obtained using 750 configurations with multiple source positions. For the connected contributions we evaluate the three-point function for five source-sink time separations, t_s/a=12, 14, 16, 18, 20 which correspond to 0.97 fm to 1.62 fm. The number of source positions increases with t_s to ensure a good quality of signal for the highest value. The total number of measurements for the aforementioned values of source- sink separation are: 3000, 4500, 12000, 24000, 24000, respectively. The inversions of the Dirac operator have been accelerated using multigrid algorithms [3]. The evaluation of the disconnected contributions requires a large number of two-point function for multiple source positions to satisfactory reduce statistical uncertainties. In this work we use 200 source positions per configuration which lead to statistically independent data given the large volume of the ensemble. For the evaluation of the up and down quark loops we use the first 200 low modes of the squared Dirac operator to reconstruct exactly a part of the loop. The contribution from the high

modes is estimated stochastically using a single noise vector per configuration, hierarchical probing, one-end trick and spin-color dilution. The parameters for the calculation of the disconnected diagram can be found in Ref [4]. The disconnected diagram requires the disconnected quark loop:

$$L(t_{\rm ins},\vec{q}) = \sum_{\vec{x}_{\rm ins}} {\rm Tr}\left[D^{-1}(x_{\rm ins};x_{\rm ins})\mathscr{G}\right] e^{+i\vec{q}\cdot\vec{x}_{\rm ins}} \tag{2.1}$$

where $D^{-1}(x_{\rm ins};x_{\rm ins})$ is the quark propagator and $\mathscr{G}$ is the Dirac structure. We employ stochastic techniques to estimate it, and due to the sparsity of the Dirac operator and its decay properties, dilution schemes are favorable. We employ the *hierarchical probing* technique [5], which allows one to eliminate stochastic noise entering from neighboring points on the lattice up to distance 2^k where $k \in \mathbb{N}$. Stochastic noise entering from points with further distance is suppressed from the properties of noise vectors: $N_r^{-1}\sum_r |\xi_r\rangle\langle\xi_r| = 1 + \mathscr{O}\left(1/\sqrt{N_r}\right)$, where N_r is the size of the stochastic ensemble. Hierarchical probing has been employed with success in previous studies with heavier pion mass ensemble (see e.g. Ref. [6]). For simulations at the physical point, the light quark propagator decays more slowly and a large probing distance is needed. One can avoid the need of increasing the distance needed by combining deflation of the low modes with hierarchical probing. In this work we reconstruct the light quark loops from the low modes of the squared Dirac operator while the contribution from the high modes is estimated stochastically. We also employ dilution in spin and color spaces, and the *one-end trick* used in our earlier studies [7, 8].

3. Nucleon Form Factor

The form factors are extracted from nucleon matrix element given by $\langle N(p',s')|\mathscr{O}_\mu^\Gamma|N(p,s)\rangle = \sqrt{\frac{m_N^2}{E_N(\vec{p}')E_N(\vec{p})}}\bar{u}_N(p',s')\Lambda_\mu^\Gamma(q^2)u_N(p,s)$, where $N(p,s)$ is the nucleon state with momentum p and spin s, energy $E_N(\vec{p})$=p_0, mass m_N. $\vec{q}$=$\vec{p}' - \vec{p}$ represents the momentum transfer, and $\mathscr{O}_\mu^\Gamma$ is the current insertion. For this work we focus on the vector ($\mathscr{O}_\Gamma$=$\bar{q}\gamma_\mu\tau^a q$) and axial ($\mathscr{O}_\Gamma$=$\bar{q}\gamma_5\gamma_\mu\tau^a q$) currents.

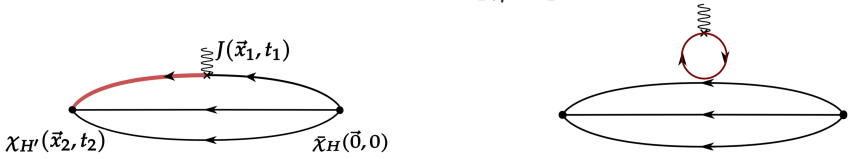

Figure 1: Connected (left) and disconnected (right) diagram required for the evaluation of the nucleon 3-point functions. The source (sink) is at x_0 (x_2) and the current insertion at x_1.

In the evaluation of quark contributions to nucleon matrix elements there are two types of diagrams, the connected and disconnected, as shown in Fig. 1. We note that in the case of the flavor isovector combination, $(u-d)$, only the connected diagram contributes. For the computation of nucleon matrix elements one needs proper 2- and 3-pt correlation functions (G^{2pt}, G^{3pt}) and then form the dimensionless ratio $R_{\mathscr{O}}$:

$$G^{2pt}(\vec{p}',t_f)=\sum_{\vec{x}_f} e^{-i\vec{x}_f\cdot\vec{p}'}\Gamma^0_{\beta\alpha}\langle J_\alpha(\vec{x}_f,t_f)\bar{J}_\beta(0)\rangle,\; G^{3pt}_{\mathscr{O}}(\Gamma^\mu,\vec{p}',t_f)=\sum_{\vec{x}_f,\vec{x}} e^{i(\vec{x}\cdot\vec{p}'-\vec{x}_f\cdot\vec{p}')}\Gamma^\mu_{\beta\alpha}\langle J_\alpha(\vec{x}_f,t_f)\mathscr{O}(\vec{x},t)\bar{J}_\beta(0)\rangle\,, \tag{3.1}$$

$$R_{\mathscr{O}}(\Gamma,\vec{p}',t,t_f)=\frac{G^{3pt}_{\mathscr{O}}(\Gamma,\vec{p}',t)}{G^{2pt}(\vec{0},t_f)}\times\sqrt{\frac{G^{2pt}(-\vec{p}',t_f-t)G^{2pt}(\vec{0},t)G^{2pt}(\vec{0},t_f)}{G^{2pt}(\vec{0},t_f-t)G^{2pt}(-\vec{p}',t)G^{2pt}(-\vec{p}',t_f)}}\underset{\substack{t_f-t\to\infty\\ t-t_i\to\infty}}{\to}\Pi(\Gamma,\vec{p}')\,. \tag{3.2}$$

The usual method to extract data is to seek for a plateau with respect to the operator insertion time, t (or alternatively t_s), which must be located at a time well separated from the source and

sink to ensure single state dominance. We also employ alternative analysis techniques to control excited states contaminations, such as 2-state fits and the summation method, using multiple t_s values ($12a-20a$ in this work). Renormalized matrix elements can be parameterized in terms of generalized form factors. The vector current decomposes into the Dirac (F_1) and Pauli (F_2) form factors, while the axial current yields the axial (G_A) and induced-pseudoscalar (G_p):

$$\Lambda^V_\mu(q^2) = \gamma_\mu F_1(q^2) + \frac{i\sigma_{\mu\nu}q^\nu}{2m_N}F_2(q^2), \quad \Lambda^A_\mu(q^2) = \frac{i}{2}\gamma_5\gamma_\mu G_A(q^2) + \frac{q_\mu\gamma_5}{2m_N}G_p(q^2)\,. \tag{3.3}$$

The Dirac and Pauli form factors can also be expressed in terms of the nucleon electric G_E and magnetic G_M Sachs form factors via $G_E(q^2) = F_1(q^2) + \frac{q^2}{(2m_N)^2}F_2(q^2)$ and $G_M(q^2) = F_1(q^2) + F_2(q^2)$.

3.1 Electromagnetic Form Factors

In Fig. 2 we present a demonstration of the excited states investigations for the isovector electromagnetic form factors. The data correspond to Q^2=0.216 GeV^2 and include the points from the plateau method for t_s/a=16, 18, 20 shown with blue circles, green squares and red triangles, respectively. The ground-state value extracted from the two-state fit is shown with a gray band. We find that the ratio for G_E (upper panel) shows a trend to lower values with t_s/a=20 becoming compatible with the value extracted from the two-state fit. For G_M (lower panel) the value extracted from the two-state fit is compatible with the ratio indicating no excited states.

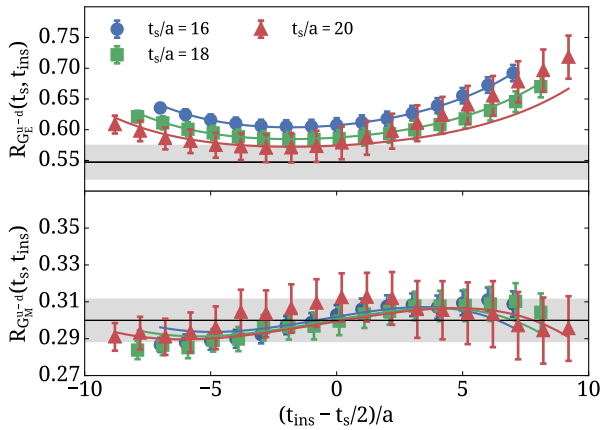

Figure 2: Results showing the plateau values and two-state simultaneous fits for G_E^{u-d} (upper panel) and G_M^{u-d} (lower panel) at Q^2=0.216 GeV^2. The results from the ratio for t_s/a=16, 18, 20 are shown with blue circles, green squares and red triangles, respectively. The gray horizontal band is the extracted value of the ground state using the two-state fit method.

The momentum transfer dependence of the electromagnetic form factors may be fitted assuming a dipole Ansatz $G_{E,M}(Q^2)$=$G_{E,M}(0)/(1+Q^2/M^2_{E,M})^2$ where $G_E(0)$ gives the electric charge and $G_M(0)$ the magnetic moment, μ. The electric and magnetic mean square radii can then be extracted from $\langle r^2\rangle$=$12/M^2$. An alternative fit form that has been used on experimental data of both electromagnetic and axial form factors is the model independent z-expansion, and we also use it for our lattice data. In this case, the form factor is expanded in a series given by $G(Q^2)$=$\sum_{k=0}^{k_{\rm max}} a_k z^k$, z=$\frac{\sqrt{t_{\rm cut}+Q^2}-\sqrt{t_{\rm cut}}}{\sqrt{t_{\rm cut}+Q^2}+\sqrt{t_{\rm cut}}}$ where $t_{\rm cut}$=$4m_\pi^2$ is the time-like cut of the isovector form factor. The series is truncated until convergence is reached at some $k_{\rm max}$ (typically 3-4) [9]. In this case, $G(0)$=a_0, while the mean square radius is given by $\langle r^2\rangle = -3a_1/2a_0t_{cut}$.

The isovector electromagnetic Sachs form factors are shown in Fig. 3 for the largest separation and the dipole form and the z-expansion with green and red bands, respectively. Both fit forms describe very well our data for G_E (left), which lie, however, about one to two standard deviations above the experimental parameterization (black line). For G_M the dipole and z-expansion fits are in good agreement with the experimental parameterization in the range Q^2>0.15 GeV^2, while for

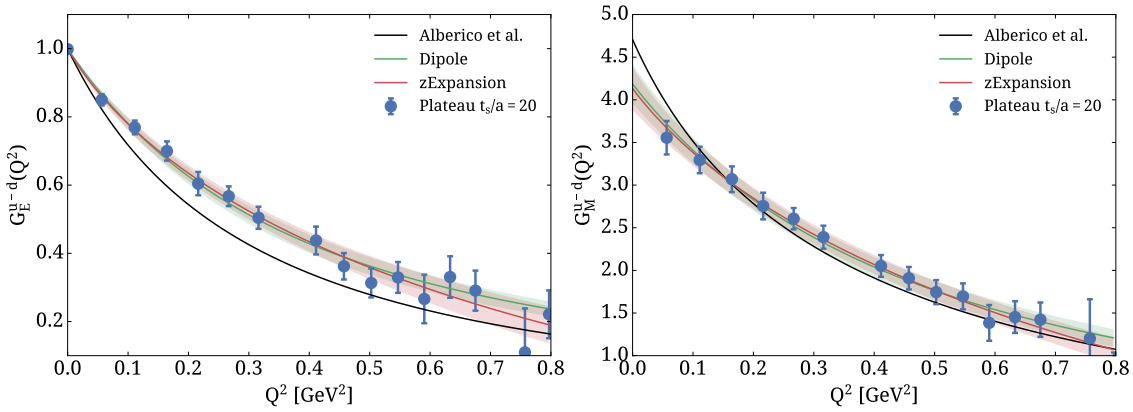

Figure 3: G_E^{u-d} (left) and G_M^{u-d} (right) for t_s/a=20 (blue circles) as a function of Q^2. Fits of the Q^2 dependence are shown for the dipole form (green band) and z-expansion (red band) for $k_{\max}$=4. The black solid line is the parameterization of the experimental data [10].

Q^2<0.15 GeV^2 our fits are lower. This could be due to pion cloud effects that are more prominent for small momenta. Detailed analysis on the connected and disconnected contributions for the electromagnetic form factors and their derived quantities can be found in Ref. [4].

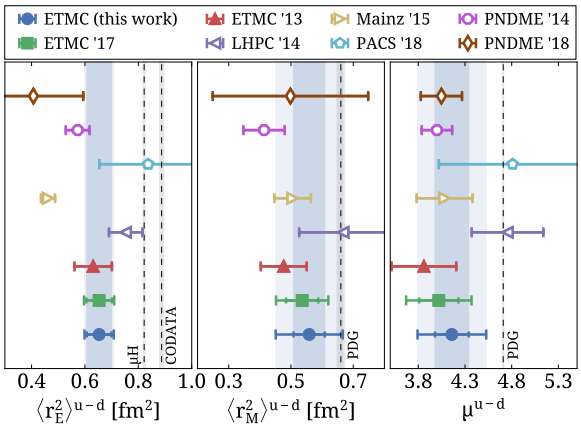

Figure 4: Results for $\langle r_E^2 \rangle^{u-d}$, $\langle r_M^2 \rangle^{u-d}$ and μ^{u-d} from this work (blue filled circles with blue vertical bands for the uncertainties), compared to our previous studies using N_f=2 at m_π=130 MeV (green filled squares) and m_π=213 MeV(red filled upper triangles). Results from other collaborations are shown with open symbols: LHPC (m_π=149 MeV), Mainz (m_π=193 MeV), PACS (m_π=146MeV) and PNDME (m_π=220 MeV), (m_π=135 MeV). The vertical dashed lines denote experimental result. For references see Ref. [4].

Data on $\langle r_E^2 \rangle^{u-d}$, $\langle r_M^2 \rangle^{u-d}$ and μ^{u-d}, are shown in Fig. 4, including results from other lattice formulations, as given in the caption. The results for $\langle r_E^2 \rangle^{u-d}$ using various ensembles of twisted mass fermions [11, 12] are in good agreement, and compatible with LHPC, PNDME and PACS within uncertainties. However, the Mainz results are lower than other formulations. For $\langle r_M^2 \rangle^{u-d}$ all lattice results are in agreement and compatible with the the PDG value. Most of the results for μ^{u-d} slightly underestimate the PDG value, while LHPC and PACS are compatible with the PDG value but higher than other lattice results.

The disconnected contributions to G_E^{u+d} and G_M^{u+d} are shown in Fig. 5 using selected values of t_s for clarity purposes. Using the specialized techniques for disconnected diagrams mentioned in Section 2 the resulting statistical accuracy is well within 20% for the values shown in the figure, which is impressive given that we are using a physical pion mass ensemble.We find that the disconnected G_E^{u+d} (G_E^s) is at the per cent (per mil) level of the connected isoscalar contribution. The equivalent disconnected contributions to G_M are one order of magnitude higher than for G_E, with clear negative contribution lowering the total G_M value.

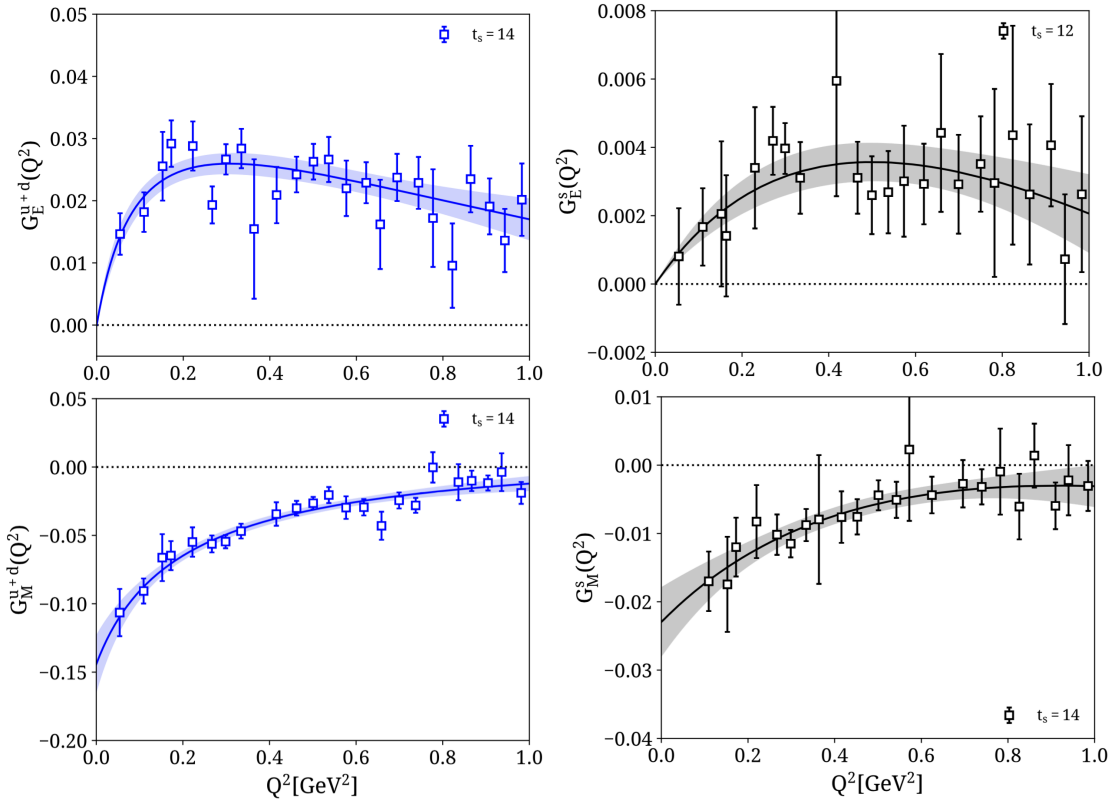

Figure 5: Results on the disconnected contributions to G_E (upper panels) and G_M (lower panels). The light (strange) quark contributions are shown with blue (black) points in the left (right) panels.

3.2 Axial Form Factors

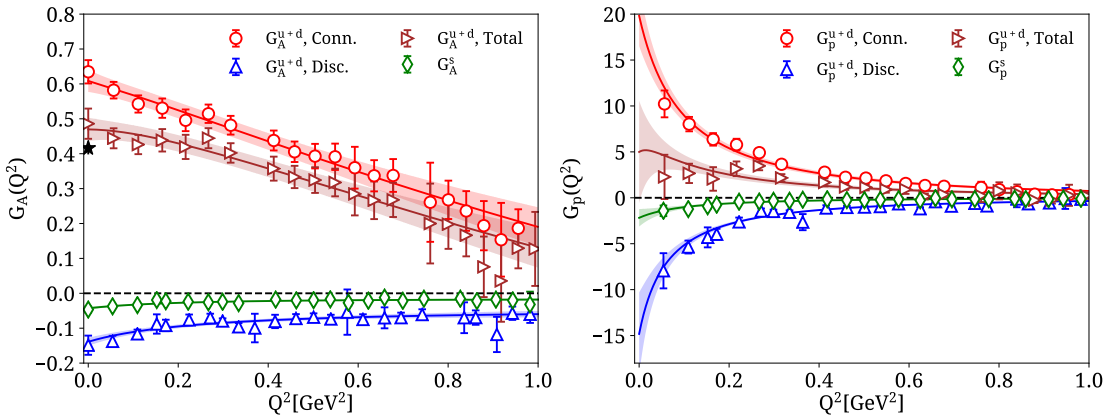

Figure 6: Results on the disconnected contributions to G_E (upper panels) and G_M (lower panels). The light (strange) quark contributions are shown with blue (black) points in the left (right) panels.

The light and strange quark contributions to G_A and G_p are shown in Fig. 6. In the same plot we show the connected (red circles), disconnected light (blue up triangles) and strange (green diamonds) contributions. The total contribution is also shown (maroon right triangles), and we find that the disconnected contributions have notable effect in both form factors. $G_p^{u+d,DI}$ is large and negative, weakening the pion-pole behavior of the connected diagram, leaving a less prominent dependence on Q^2. Fits to a z-expansion for G_A and assuming pion-pole dominance for G_p ($=G_A(Q^2)C/(1+Q^2/m_\pi^2)$) are shown with bands. The total contribution to g_A^{u+d} is compatible with

the experimental value (black star) only upon inclusion of the disconnected contributions.

Acknowledgments: We would like to thank all members of ETMC for a very constructive and enjoyable collaboration. The authors gratefully acknowledge the Gauss Centre for Supercomputing e.V. for funding this project by providing computing time on the GCS Supercomputer SuperMUC at Leibniz Supercomputing Centre. This work was supported by a grant from the Swiss National Supercomputing Centre (CSCS) under project ID s702 This project has received funding from the European Union?s Horizon 2020 research and innovation programme under grant agreement No? 642069. S. B. was supported by this program. M.C. acknowledges financial support by the U.S. National Science Foundation under Grant No. PHY-1714407. A.V acknowledges financial support by the U.S. National Science Foundation under grant PHY14-14614.

References

[1] R. Frezzotti and G. C. Rossi, "Chirally improving Wilson fermions. 1. O(a) improvement," *JHEP*, vol. 08, p. 007, 2004.

[2] C. Alexandrou *et al.*, "Simulating twisted mass fermions at physical light, strange and charm quark masses," 2018.

[3] C. Alexandrou, S. Bacchio, J. Finkenrath, A. Frommer, K. Kahl, and M. Rottmann, "Adaptive Aggregation-based Domain Decomposition Multigrid for Twisted Mass Fermions," *Phys. Rev.*, vol. D94, no. 11, p. 114509, 2016.

[4] C. Alexandrou *et al. in preparation*.

[5] A. Stathopoulos, J. Laeuchli, and K. Orginos, "Hierarchical probing for estimating the trace of the matrix inverse on toroidal lattices," 2013.

[6] J. Green, N. Hasan, S. Meinel, M. Engelhardt, S. Krieg, J. Laeuchli, J. Negele, K. Orginos, A. Pochinsky, and S. Syritsyn, "Up, down, and strange nucleon axial form factors from lattice QCD," *Phys. Rev.*, vol. D95, no. 11, p. 114502, 2017.

[7] C. Alexandrou, M. Constantinou, K. Hadjiyiannakou, K. Jansen, C. Kallidonis, G. Koutsou, and A. Vaquero Aviles-Casco, "Nucleon axial form factors using N_f = 2 twisted mass fermions with a physical value of the pion mass," *Phys. Rev.*, vol. D96, no. 5, p. 054507, 2017.

[8] C. Alexandrou *et al.*, "Nucleon scalar and tensor charges using lattice QCD simulations at the physical value of the pion mass," *Phys. Rev.*, vol. D95, no. 11, p. 114514, 2017. [Erratum: Phys. Rev.D96,no.9,099906(2017)].

[9] C. Alexandrou, M. Constantinou, K. Hadjiyiannakou, K. Jansen, C. Kallidonis, G. Koutsou, and A. Vaquero Avilés-Casco, "Strange nucleon electromagnetic form factors from lattice QCD," 2018.

[10] W. M. Alberico, S. M. Bilenky, C. Giunti, and K. M. Graczyk, "Electromagnetic form factors of the nucleon: New Fit and analysis of uncertainties," *Phys. Rev.*, vol. C79, p. 065204, 2009.

[11] C. Alexandrou, M. Constantinou, K. Hadjiyiannakou, K. Jansen, C. Kallidonis, G. Koutsou, and A. Vaquero Aviles-Casco, "Nucleon electromagnetic form factors using lattice simulations at the physical point," *Phys. Rev.*, vol. D96, no. 3, p. 034503, 2017.

[12] C. Alexandrou, M. Constantinou, S. Dinter, V. Drach, K. Jansen, C. Kallidonis, and G. Koutsou, "Nucleon form factors and moments of generalized parton distributions using $N_f = 2+1+1$ twisted mass fermions," *Phys. Rev.*, vol. D88, no. 1, p. 014509, 2013.